International Journal of Smart and Nano Materials

ISSN: 1947-5411 (Print) 1947-542X (Online) Journal homepage: https://www.tandfonline.com/loi/tsnm20

Piezoelectric d_{15} shear-response-based torsion actuation mechanism: An exact 3D Saint-Venant type solution

Michael Krommer, Pelin Berik, Yury Vetyukov & Ayech Benjeddou

To cite this article: Michael Krommer, Pelin Berik, Yury Vetyukov & Ayech Benjeddou (2012) Piezoelectric d_{15} shear-response-based torsion actuation mechanism: An exact 3D Saint-Venant type solution, International Journal of Smart and Nano Materials, 3:2, 82-102, DOI: 10.1080/19475411.2011.649807

To link to this article: https://doi.org/10.1080/19475411.2011.649807

International Journal of Smart and Nano Materials
Vol. 3, No. 2, June 2012, 82–102

Taylor & Francis
Taylor & Francis Group

Piezoelectric d_{15} shear-response-based torsion actuation mechanism: An exact 3D Saint-Venant type solution

Michael Krommer[a]*, Pelin Berik[a], Yury Vetyukov[b] and Ayech Benjeddou[c]

[a]*Institute for Technical Mechanics, Johannes Kepler University Linz, Altenbergerstr.69, A-4040 Linz, Austria;* [b]*Linz Center of Mechatronics GmbH, Altenbergerstr.69, A-4040 Linz, Austria;* [c]*SUPMECA, Structures, 3 rue Fernand Hainaut - 93407 Saint Ouen CEDEX, France*

(*Received 15 October 2011; final version received 12 December 2011*)

This paper is concerned with the detailed analysis of the behavior of a piezoceramic bi-morph torsion actuator using the d_{15}-effect. The bi-morph actuator is made of two oppositely polarized adjacent piezoceramic prismatic beams. The mathematical analysis is based on the Saint-Venant torsion theory; a formulation of the electromechanically coupled problem in terms of a stress function and of the electric potential is derived, which represents an exact solution of a specific three-dimensional problem; in particular, for the case when the axial stress and the axial component of the electric displacement vector are independent of the axial coordinate. The resulting boundary–value problem in the cross-section is solved using the method of finite differences. Solutions for the actuated rate of twist are presented and compared to three-dimensional electromechanically coupled finite element solutions using ABAQUS® for the case of a cantilevered bi-morph actuator. A very good agreement is found.

Keywords: piezoelectric d_{15} - effect; bi-morph torsion actuator; exact Saint-Venant-type solution; numerical validation

1. Introduction

Structures that integrate sensors and actuators into load-bearing structures by means of multi-functional materials like, e.g. piezoelectric materials, are usually denoted as smart or intelligent structures; see Crawley [1] or Chopra [2] for reviews. In combination with active and passive control strategies smart structures have applications in the fields of vibration damping, noise reduction, shape control, structural and health monitoring, and so on; see, e.g. Rao and Sunar [3].

A piezoelectric material subjected to an electric field is mechanically deformed; conversely, a mechanical deformation results into an electric field. This behavior can be used to put piezoelectric actuators and sensors into practice. The actuator effect is denoted as the converse piezoelectric effect and the sensor effect as the direct piezoelectric effect; see Mason [4] or Yang [5]. In the following, the actuating piezoelectric strains are considered as mechanical eigenstrains, a generalized notion introduced by Mura [6] in order to describe incompatible parts of strain, such as thermal, plastic misfit as well as piezoelectric strains. In analogy, the sensing effect has been formally accounted for by means of a so-called

*Corresponding author. Email: michael.krommer@jku.at

ISSN 1947-542X online

http://dx.doi.org/10.1080/19475411.2011.649807
http://www.tandfonline.com

electrical eigenfield; this notion was introduced by Irschik *et al*. [7]. In general, problems involving piezoelectric materials are electromechanically coupled problems, which require one to account for the full field equations of mechanics and electrostatics. In the present paper, we focus on the solution of a specific problem of this type; namely a piezoelectric bi-morph torsion actuator.

Compensating or controlling torsional deformation is a necessity in many applications, such as wind turbines, helicopter blades, robot arms, flexible space structures, etc.; this can be reached indirectly via bending-twisting (Aldraihem and Wetherhold [8] or Kioua and Mirza [9]) or extension-twisting (Zhu *et al*. [10]) stiffness couplings or directly through the electromechanical coupling between an electric field that is applied through-the-thickness and torsional shear strains via the piezoelectric d_{36}-effect; see, e.g. Zehetner [11], Zehetner and Krommer [12], Tzou *et al*. [13] and Qiu *et al*. [14]. However, the latter effect is not exhibited by mono-morph piezoelectric materials rendering the direct torsional deformation sensing or actuation non-feasible; nevertheless, this coupling can be obtained indirectly using either skewed piezoelectric polymers (Tzou *et al*. [13], Qiu *et al*. [14] or Chopra [2]) due to their orthotropic piezoelectric coupling properties, or piezoceramic fiber composite actuators and sensors that were made orthotropic through a suitable fiber/epoxy blend as discussed by Aldraihem and Wetherhold [8].

In order to overcome these difficulties, research on torsion actuation using the direct d_{15}-effect of mono-morph piezoceramic materials has attracted noticeable interest since the mid-1990s; see Benjeddou [15]. This torsion actuation mechanism was achieved experimentally using tubular actuators assembled from eight segments that were cut from circumferentially polarized piezoceramic tubes (Sung *et al*. [16], Glazounov *et al*. [17] and Centolanza *et al*. [18]), and theoretically using patches symmetrically bonded to the surface of a structure and polarized in the thickness direction (Thakkar and Ganguli [19] and Pawar and Jung [20]). A benchmark was recently proposed consisting of a slender cantilever beam comprising two piezoceramic layers with opposite polarization along their length and perfectly bonded along their width by Butz *et al*. [21]. This concept was experimentally proven by Berik and Benjeddou [22] for a cantilever plate consisting of two identical glass fiber/epoxy faces sandwiching a core torsion actuator; the latter mimics the benchmark by using a total of six segmented d_{15} piezoceramic patches. Yet, a thorough mathematical analysis of this electromechanically coupled problem has not been reported; the latter is the topic of the present paper.

In Section 2, we summarize the basic equations of the linearized theory of piezoelasticity in some detail. In particular, the d_{15}-effect of mono-morph piezoceramic materials is discussed and an exact analytical solution for a kinematically unconstrained actuator is presented. Finally, the bi-morph configuration studied in this paper is introduced. Section 3 discusses the details of the mathematical analysis of the electromechanically coupled problem; stress, strain, deformation and electric field are considered in this analysis. A numerical example is presented in Section 4; a finite difference solution of the presented formulation is discussed and numerical results are shown. Finally, the latter results are compared to results computed with three-dimensional electromechanically coupled finite elements.

2. Piezoelectric materials exhibiting the d_{15}-effect

Before we focus on the use of piezoelectric materials exhibiting the d_{15}-effect (such as materials with crystal symmetry 6mm that are polarized in an in-plane direction) to put a torsion actuator into practice, we will briefly discuss the fundamental relations and behavior of these materials in some detail. In order to characterize the response, we consider a

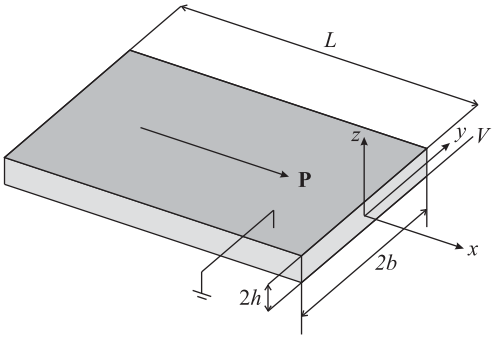

Figure 1. Sketch of a mono-morph d_{15} shear piezoelectric actuator.

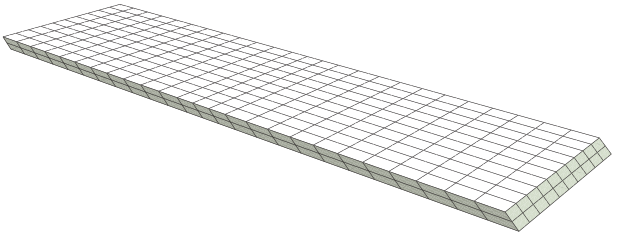

Figure 2. Deformation of a mono-morph d_{15} shear piezoelectric actuator.

thin plate with electrodes at the horizontal surfaces and with an applied electric potential difference between the electrodes as shown in Figure 1. No mechanical loading is applied and the plate is kinematically unconstrained, other than to prohibit a rigid body motion. The resulting deformation due to the applied electric potential difference is shown in Figure 2. One can see from this figure that the mono-morph actuator results in a deformation, for which the strain tensor is homogeneous. In particular, we have a pure transverse shear strain $\boldsymbol{\varepsilon} = e_0(\mathbf{e}_x\mathbf{e}_z + \mathbf{e}_z\mathbf{e}_x)$, with a constant e_0, if the material is polarized in the x-direction, as shown in Figure 1.

The constitutive relations for a material, which is polarized in the x-direction, formulated in a coordinate system, for which the coordinate axes coincide with the principal material axes, are

$$\begin{bmatrix} \sigma_{xx} \\ \sigma_{yy} \\ \sigma_{zz} \\ \sigma_{yz} \\ \sigma_{xz} \\ \sigma_{xy} \end{bmatrix} = \begin{bmatrix} C_{33} & C_{13} & C_{13} & 0 & 0 & 0 \\ C_{13} & C_{11} & C_{12} & 0 & 0 & 0 \\ C_{13} & C_{12} & C_{11} & 0 & 0 & 0 \\ 0 & 0 & 0 & C_{66} & 0 & 0 \\ 0 & 0 & 0 & 0 & C_{55} & 0 \\ 0 & 0 & 0 & 0 & 0 & C_{55} \end{bmatrix} \begin{bmatrix} \varepsilon_{xx} \\ \varepsilon_{yy} \\ \varepsilon_{zz} \\ \gamma_{yz} \\ \gamma_{xz} \\ \gamma_{xy} \end{bmatrix} - \begin{bmatrix} e_{33} & 0 & 0 \\ e_{31} & 0 & 0 \\ e_{31} & 0 & 0 \\ 0 & 0 & 0 \\ 0 & 0 & e_{15} \\ 0 & e_{15} & 0 \end{bmatrix} \begin{bmatrix} E_x \\ E_y \\ E_z \end{bmatrix},$$

with $C_{66} = \frac{1}{2}(C_{11} - C_{12})$,

$$\begin{bmatrix} D_x \\ D_y \\ D_z \end{bmatrix} = \begin{bmatrix} \in_{33} & 0 & 0 \\ 0 & \in_{11} & 0 \\ 0 & 0 & \in_{11} \end{bmatrix} \begin{bmatrix} E_x \\ E_y \\ E_z \end{bmatrix} + \begin{bmatrix} e_{33} & e_{31} & e_{31} & 0 & 0 & 0 \\ 0 & 0 & 0 & 0 & 0 & e_{15} \\ 0 & 0 & 0 & 0 & e_{15} & 0 \end{bmatrix} \begin{bmatrix} \varepsilon_{xx} \\ \varepsilon_{yy} \\ \varepsilon_{zz} \\ \gamma_{yz} \\ \gamma_{xz} \\ \gamma_{xy} \end{bmatrix}. \quad (1)$$

In the remainder of this paper we will be using a direct tensor notation (see, e.g. Lurie [23]); within the framework of this notation, the constitutive relations can be reformulated as

$$\boldsymbol{\sigma} = \mathbf{C} \cdot\cdot \boldsymbol{\varepsilon} - \mathbf{e} \cdot \mathbf{E}, \quad \mathbf{D} = \boldsymbol{\epsilon} \cdot \mathbf{E} + \mathbf{e} \cdot\cdot \boldsymbol{\varepsilon}. \tag{2}$$

Here, $\boldsymbol{\sigma}$ is is the second-rank symmetric stress tensor, $\boldsymbol{\varepsilon}$ is the second-rank symmetric strain tensor, $\mathbf{D}$ is the electric displacement vector and $\mathbf{E}$ is the electric field vector. $\mathbf{C}$ denotes the fourth-rank elasticity tensor at constant electric field, $\mathbf{e}$ is the third-rank tensor of piezoelectric stress coefficients and $\boldsymbol{\epsilon}$ is the second-rank permittivity tensor at constant strain. In many problems we prefer to introduce a second-rank eigenstrain tensor $\boldsymbol{\varepsilon}^*$, such that the mechanical constitutive relations can be reformulated as

$$\boldsymbol{\sigma} = \mathbf{C} \cdot\cdot \left(\boldsymbol{\varepsilon} - \boldsymbol{\varepsilon}^*\right), \quad \textit{with}: \ \boldsymbol{\varepsilon}^* = \underbrace{\mathbf{C}^{-1} \cdot\cdot \mathbf{e}}_{=\mathbf{d}} \cdot \mathbf{E} = \mathbf{d} \cdot \mathbf{E}. \tag{3}$$

The matrix of components of the newly introduced third-rank tensor $\mathbf{d}$ is

$$[\mathbf{d}]^T = \begin{bmatrix} d_{33} & 0 & 0 \\ d_{31} & 0 & 0 \\ d_{31} & 0 & 0 \\ 0 & 0 & 0 \\ 0 & 0 & d_{15} \\ 0 & d_{15} & 0 \end{bmatrix}. \tag{4}$$

The general notion of eigenstrains $\boldsymbol{\varepsilon}^*$ was introduced by Mura [6] for incompatible strains; plastic misfit strains, thermal strains or piezoelectric strains are just a few examples for such eigenstrains. An alternative notion refers to such sources of mechanical deformations or stresses as sources of self-stress; see the classical papers by Reissner [24] and Nemenyi [25]. In the present paper the well-known analogy between thermal expansion strains and piezoelectric strains – see, e.g. Vinson [26] – is of particular importance. It is well known that certain temperature distributions in kinematically unconstrained bodies do not result into any stress; in case of an isotropic and isothermal problem such temperature distributions must be linear with respect to the spatial coordinates; see Hetnarski [27] for a proof. For the case of general eigenstrains in anisotropic bodies this latter result can be extended and it follows that the linearity of the eigenstrain tensor $\boldsymbol{\varepsilon}^*$ with respect to the spatial coordinates is sufficient for compatibility.

Next, we summarize the governing equations, other than the constitutive relations; moreover, we will use the set of governing equations to prove that the deformation of a d_{15} actuator as presented in Figure 2 can be easily computed analytically; the result shown in the figure was computed using three-dimensional electromechanically coupled finite elements. The mechanical equilibrium conditions and boundary conditions are

$$\nabla \cdot \boldsymbol{\sigma} = 0, \ \boldsymbol{\sigma} \cdot \mathbf{e}_n = 0, \tag{5}$$

if the boundary of the body is stress-free. These equations are satisfied identically for $\boldsymbol{\sigma} = \mathbf{0}$. Then, the mechanical constitutive relations result in $\boldsymbol{\varepsilon} = \boldsymbol{\varepsilon}^* = \mathbf{d} \cdot \mathbf{E}$, which is a possible solution for the strain tensor as long as $\mathbf{d} \cdot \mathbf{E}$ is compatible. Hence, the compatibility conditions

$$\Delta\boldsymbol{\varepsilon} + \nabla\nabla tr\boldsymbol{\varepsilon} = 2(\nabla\nabla\cdot\boldsymbol{\varepsilon})^S \tag{6}$$

must be satisfied. As we have already discussed, this is the case if the eigenstrain tensor $\boldsymbol{\varepsilon}^* = \mathbf{d}\cdot\mathbf{E}$ is linear with respect to the spatial coordinates. We proceed with the electrical equations. From the constitutive relation with $\boldsymbol{\sigma} = \mathbf{0}$ we find that

$$\mathbf{D} = \boldsymbol{\epsilon}\cdot\mathbf{E} + \mathbf{e}\cdot\cdot\boldsymbol{\varepsilon} = (\boldsymbol{\epsilon} + \mathbf{e}\cdot\cdot\mathbf{d})\cdot\mathbf{E} = \boldsymbol{\eta}\cdot\mathbf{E}. \tag{7}$$

Then, the charge equation of electrostatics

$$\nabla\cdot\mathbf{D} = \mathbf{0} \tag{8}$$

is satisfied if $\boldsymbol{\eta}\cdot\mathbf{E}$ is constant, which is the case for $\mathbf{E} = (V/2h)\mathbf{e}_z$; see Figure 1. Here, V is the applied electric potential difference and $2h$ is the thickness of the piezoelectric plate; $\mathbf{e}_z$ is the unit vector in the thickness direction. Moreover, $\mathbf{D} = \boldsymbol{\eta}\cdot\mathbf{e}_z(V/2h)$ is a vector pointing in the thickness direction (this follows directly from the constitutive relation for the d_{15} actuator), such that the boundary conditions at the vertical boundaries, $\mathbf{D}\cdot\mathbf{e}_n = 0$, are satisfied and the fact that the electric field vector in electrostatics must be irrotational,

$$\nabla\times\mathbf{E} = \mathbf{0}, \tag{9}$$

holds. Finally, the equipotential area condition for the electrodes is satisfied, because $\mathbf{E} = (V/2h)\mathbf{e}_z$ is constant; also, the compatibility conditions are satisfied. Hence, the analytical solution of the d_{15} mono-morph actuator for the mechanical and electrical fields is

$$\boldsymbol{\sigma} = \mathbf{0}\,,\ \boldsymbol{\varepsilon} = d_{15}\frac{V}{2h}\left(\mathbf{e}_x\mathbf{e}_z + \mathbf{e}_z\mathbf{e}_x\right)\,,\ \mathbf{E} = \frac{V}{2h}\mathbf{e}_z\,,\ \mathbf{D} = \eta_{11}\frac{V}{2h}\mathbf{e}_z. \tag{10}$$

From this solution we identify the previously introduced e_0 as $e_0 = d_{15}(V/2h)$. The reason the exact analytical solution can be derived easily, is the fact that the eigenstrain is compatible and that no external forces act on the body. Recently, Berik and Benjeddou [28] have reported experimental and numerical results for the case when such shear actuators are used as the core of a sandwich structure.

A different problem appears for a bi-morph configuration as shown in Figure 3. Here two mono-morph d_{15} actuators, which are polarized in opposite directions, are perfectly bonded to each other along one of their vertical faces parallel to the polarization direction. The horizontal surfaces are totally electroded. Due to the opposite polarization direction the eigenstrain tensor is no longer compatible, because it exhibits a jump at the interface, at which the two actuators are bonded to each other. Hence, the solution of the problem is far less trivial.

The deformation (computed using three-dimensional electromechanically coupled finite elements) of a bi-morph d_{15} actuator for an applied electric potential difference is shown in Figure 4. The mathematical analysis of this torsion problem in combination with a numerical verification is the topic of this paper.

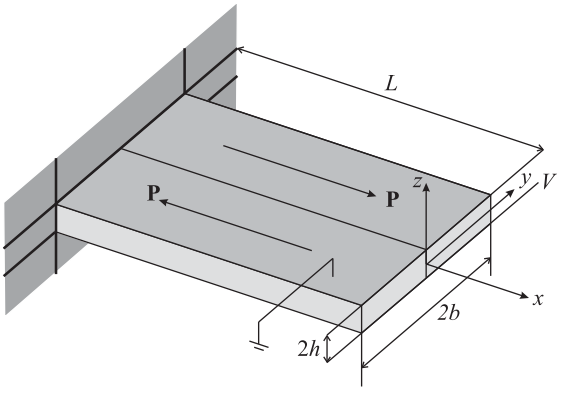

Figure 3. Sketch of a bi-morph d_{15} piezoceramic torsion actuator.

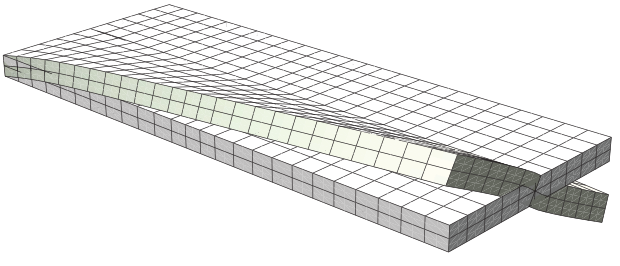

Figure 4. Deformation of a bi-morph d_{15} piezoceramic torsion actuator.

3. Analysis of a bi-morph d_{15} torsion actuator

In this section, we present the mathematical analysis of the problem of a bi-morph d_{15} torsion actuator as shown in Figure 3. In particular, we seek a solution of the three-dimensional electromechanically coupled problem, which is independent of the axial coordinate. In other words, we seek to extend the classical analysis of the Saint-Venant problem of unconstrained torsion of a straight prismatic beam with respect to the effect of piezoelectric eigenstrains. In the course of the analysis we follow the derivations as given by Eliseev [29], as far as they are concerned with the mechanical part of the problem; the analysis of the electrical part completes this section.

3.1. Constitutive relations

We start the analysis with the discussion of those parts of the constitutive relations that are sufficient for the present problem. The stress tensor and the electric displacement vector can be written as

$$\begin{aligned} \boldsymbol{\sigma} &= \sigma_{xx}\mathbf{e}_x + \boldsymbol{\tau}\mathbf{e}_x + \mathbf{e}_x\boldsymbol{\tau} + \boldsymbol{\sigma}_2, \\ \mathbf{D} &= D_x\mathbf{e}_x + \mathbf{D}_2. \end{aligned} \tag{11}$$

In Equation (11), $\mathbf{e}_x$ is the unit vector in the axial direction, σ_{xx} is the normal stress in the axial direction, $\boldsymbol{\tau}$ is the shear stress vector in the cross-section and $\boldsymbol{\sigma}_2$ is the plane stress tensor in the cross-section. D_x is the axial component of the electric displacement vector

and $\mathbf{D}_2$ refers to the projection of the electric displacement vector into the cross-sectional plane. As we are interested in solutions that are independent of the axial coordinate x, $\boldsymbol{\tau}$ and $\mathbf{D}_2$ are the entities we are interested in in the analysis. The constitutive relations follow from Equation (2) in the form:

$$\underbrace{\begin{bmatrix}\sigma_{xy}\\ \sigma_{xz}\end{bmatrix}}_{[\boldsymbol{\tau}]} = G\underbrace{\begin{bmatrix}\gamma_{xy}\\ \gamma_{xz}\end{bmatrix}}_{[\boldsymbol{\gamma}]} - e\underbrace{\begin{bmatrix}E_y\\ E_z\end{bmatrix}}_{[\mathbf{E}_2]}, \underbrace{\begin{bmatrix}D_y\\ D_z\end{bmatrix}}_{[\mathbf{D}_2]} = \in \underbrace{\begin{bmatrix}E_y\\ E_z\end{bmatrix}}_{[\mathbf{E}_2]} + e\underbrace{\begin{bmatrix}\gamma_{xy}\\ \gamma_{xz}\end{bmatrix}}_{[\boldsymbol{\gamma}]}. \tag{12}$$

In Equation (12) we have introduced the shear strain vector $\boldsymbol{\gamma}$, the shear modulus $G = C_{55}$, the piezoelectric coefficient $e = e_{15}$ and the permittivity $\in = \in_{11}$. In terms of our preferred direct tensor notation we have

$$\boldsymbol{\tau} = G\boldsymbol{\gamma} - e\mathbf{E}_2 = G\left(\boldsymbol{\gamma} - \boldsymbol{\gamma}^*\right), \quad \mathbf{D}_2 = \in \mathbf{E}_2 + e\boldsymbol{\gamma}. \tag{13}$$

In Equation (13), $\boldsymbol{\gamma}^* = (e/G)\mathbf{E}_2$ is the so-called shear eigenstrain vector. Note that the vectors in Equation (13) are vectors in a three-dimensional Euclidean space; yet, their component in the axial direction is trivial. If we wish to refer to the components we do not explicitly write the trivial component, but rather use the notation $[\mathbf{v}] = \begin{bmatrix}v_y & v_z\end{bmatrix}^T$; see also Equation (12).

3.2. Solution of the 3D electromechanically coupled problem

As we have already mentioned, we seek a solution of the three-dimensional problem, which does not depend on the axial coordinate. From a mechanical point of view, we follow the Saint-Venant theory of unconstrained torsion with a special emphasis on the influence of a shear eigenstrain, $\boldsymbol{\tau} = G(\boldsymbol{\gamma} - \boldsymbol{\gamma}^*)$. We note that the problem we are analyzing here is an electromechanically coupled problem, which requires us to account for both, the mechanical and the electrical field equations; the two fields are coupled via the constitutive relations.

3.2.1. Analysis of stress

We assume a particular solution of the three-dimensional equilibrium conditions $\nabla \cdot \boldsymbol{\sigma} = \mathbf{0}$, which is independent of the axial coordinate, in the form

$$\sigma_{xx} = 0\,, \quad \boldsymbol{\sigma}_2 = \mathbf{0}\,, \quad \boldsymbol{\tau} = \nabla_2\phi \times \mathbf{e}_x. \tag{14}$$

Here, we denote the two-dimensional differential operator as ∇_2 and $\phi = \phi(\mathbf{z})$ is a stress function. $\mathbf{z}$ is the position vector of an arbitrary point in the cross-section relative to the beam axis. The stress tensor, as introduced in Equation (14), satisfies the equilibrium conditions. The boundary conditions of the three-dimensional problem, $\boldsymbol{\sigma} \cdot \mathbf{e}_n = \mathbf{0}$, are only satisfied partially. At the boundary ∂A of any cross-section A all boundary conditions are satisfied; with the unit outer normal vector $\mathbf{n}$ of the boundary ∂A, $\boldsymbol{\sigma}_2 \cdot \mathbf{n} = \mathbf{0}$ holds. The condition $\boldsymbol{\tau} \cdot \mathbf{n} = 0$ is satisfied, if

$$\partial A: \quad \boldsymbol{\tau} \cdot \mathbf{n} = (\nabla_2\phi \times \mathbf{e}_x) \cdot \mathbf{n} = \mathbf{s} \cdot \nabla_2\phi = 0 \;\rightarrow\; \phi = 0, \tag{15}$$

because we are dealing with a simply connected cross-section. $\mathbf{s}$ is the unit tangential vector of the boundary ∂A. At the two ends of the rod, say $x = 0$ and $x = L$, the normal stress σ_{xx} and the shear stress vector $\boldsymbol{\tau}$ must vanish. The first condition is satisfied as $\sigma_{xx} = 0$; yet, the shear stress vector $\boldsymbol{\tau} = \nabla_2\phi \times \mathbf{e}_x$ is not trivial. On the other hand, we will be calculating solutions for $\boldsymbol{\tau}$, for which the resultant shear force and axial moment will at least satisfy the dynamical boundary conditions in an integral sense. In the light of the principle of Saint-Venant for statically equivalent force systems (see Ziegler [30]), we conclude that the deviation of the shear stress distribution from zero only affects the solution in the vicinity of the two ends of the rod. Hence, the solution we are discussing in the following must be understood within this context as one that is valid everywhere, other than in the vicinity of the ends of the structure; this is also true for the case of kinematical boundary conditions at these ends.

We cannot derive any further equations from the equilibrium conditions and the boundary conditions. Hence, it remains to derive an equation from which the stress function can be computed, a task for which we will utilize the compatibility conditions.

3.2.2. Analysis of strain

We proceed by deriving the governing partial differential equation for the stress function from the compatibility condition for the strain tensor, which for our specific problem, with the only non-vanishing stresses being the shear stresses in the cross-section, has the form $2\boldsymbol{\varepsilon} = \boldsymbol{\gamma}\mathbf{e}_x + \mathbf{e}_x\boldsymbol{\gamma}$. Hence, the general compatibility conditions, see Equation (6), reduce to

$$\nabla_2 (\nabla_2 \cdot \boldsymbol{\gamma}) - \Delta_2\boldsymbol{\gamma} = \nabla_2 (\nabla_2 \times \boldsymbol{\gamma} \cdot \mathbf{e}_x) \times \mathbf{e}_x = \mathbf{0}. \tag{16}$$

Equation (16) can be integrated and we find

$$\nabla_2 \times \boldsymbol{\gamma} \cdot \mathbf{e}_x = 2\alpha. \tag{17}$$

In Equation (17), α is an arbitrary constant, which at this point has no other meaning than that of an integration constant. The constitutive relation in the form $\boldsymbol{\gamma} = \frac{1}{G}\boldsymbol{\tau} + \boldsymbol{\gamma}^*$ and the representation of the shear stress vector by means of the stress function, $\boldsymbol{\tau} = \nabla_2\phi \times \mathbf{e}_x$, are inserted into Equation (17) and a Poisson equation for the stress function is obtained. Together with the homogeneous Dirichlet boundary conditions, we derive the boundary-value problem for the stress function as

$$\begin{aligned} A: &\quad \Delta_2\phi = -2G\alpha + G\mathbf{e}_x \cdot \left(\nabla_2 \times \boldsymbol{\gamma}^*\right), \\ \partial A: &\quad \phi = 0. \end{aligned} \tag{18}$$

The right-hand side of the Poisson equation in Equation (18) depends on the constant α and the piezoelectric actuation via the unknown electric field vector $\mathbf{E}_2$ by means of $\boldsymbol{\gamma}^* = (e/G)\mathbf{E}_2$. Therefore, we proceed with the problem of assigning a mechanical meaning to α and to compute the electric field vector.

3.2.3. Analysis of deformation

The strain tensor in our problem has the form $\boldsymbol{\varepsilon} = (\boldsymbol{\gamma}\mathbf{e}_x + \mathbf{e}_x\boldsymbol{\gamma})/2$; in general it is $\boldsymbol{\varepsilon} = \varepsilon_{xx}\mathbf{e}_x\mathbf{e}_x + (\boldsymbol{\gamma}\mathbf{e}_x + \mathbf{e}_x\boldsymbol{\gamma})/2 + \boldsymbol{\varepsilon}_2$. Here, ε_{xx} is the axial strain and $\boldsymbol{\varepsilon}_2$ stands for the plane strain tensor in the cross-sectional plane. Hence, the latter two parts of the strain tensor must vanish. We write the displacement vector as $\mathbf{u} = u_x\mathbf{e}_x + \mathbf{v}$, in which u_x denotes the axial

displacement and $\mathbf{v}$ the displacements normal to the beam axis. The components of the displacement vector are in general functions of the axial coordinate x and the position of a point in the cross-section, defined by the previously introduced vector $\mathbf{z}$. From the vanishing of certain components of the strain tensor we find

$$\begin{aligned} \varepsilon_{xx} = 0 \quad &\rightarrow \quad u_x(x,\mathbf{z}) = U(\mathbf{z}), \\ \boldsymbol{\varepsilon}_2 = \mathbf{0} \quad &\rightarrow \quad (\nabla_2 \mathbf{v})^S = \mathbf{0} \quad \rightarrow \quad \mathbf{v}(x,\mathbf{z}) = \mathbf{V}(x) + \omega(x)\mathbf{e}_x \times \mathbf{z}. \end{aligned} \tag{19}$$

The displacement field in Equation (19) corresponds to a rigid body motion of a cross-section with a superposed axial displacement, which does not depend on the axial coordinate x; the latter is called axial warping and is accounted for by $U(\mathbf{z})$. The rigid body motion consists of a translation of points on the axis $\mathbf{V}(x)$ and a rotation of the cross-section described by the twisting angle $\omega(x)$.

Next, we compute the shear strain vector in two ways: (1) from the constitutive relation $\boldsymbol{\gamma} = \frac{1}{G}\boldsymbol{\tau} + \boldsymbol{\gamma}^*$ and (2) from the displacement field $\boldsymbol{\gamma} = \nabla_2 U + \frac{\partial}{\partial x}\mathbf{v}$. From these two formulations we find that

$$\boldsymbol{\tau} + G\boldsymbol{\gamma}^* = \nabla_2\phi \times \mathbf{e}_x + G\boldsymbol{\gamma}^* = G\nabla_2 U + G\frac{d}{dx}\mathbf{V} + G\frac{d\omega}{dx}\mathbf{e}_x \times \mathbf{z}. \tag{20}$$

Note that we have inserted the definition of the shear stress vector by means of the stress function. As we are in particular interested in assigning a mechanical meaning to the constant α, we apply $\nabla_2\times$ to the last relation. The first two terms of the right-hand side are identically zero and from the remaining terms we derive

$$\left(-\Delta_2\phi + G\mathbf{e}_x \cdot \nabla_2 \times \boldsymbol{\gamma}^* - 2G\frac{d\omega}{dx}\right)\mathbf{e}_x = \mathbf{0}. \tag{21}$$

Finally, we account for the Poisson equation $\Delta_2\phi = -2G\alpha + G\mathbf{e}_x \cdot (\nabla_2 \times \boldsymbol{\gamma}^*)$ from Equation (18), which results in

$$\alpha = \frac{d\omega}{dx}. \tag{22}$$

This is a well-known result from torsion theory for elastic rods; α is the rate of twist, which is the derivative of the twisting angle ω with respect to the axial coordinate x. We have derived this result in detail here, as we believe it cannot be directly concluded for torsion problems with eigenstrains. Likewise, the next step would be to discuss the solution for the warping function $U(\mathbf{z})$. However, for the goal of the present paper this is not needed and we will study this problem elsewhere. It is in general interesting, as there is a discussion in the literature, whether the warping function for problems with piezoelectric eigenstrains is identical to the elastic one or not.

3.2.4. Analysis of electrical equations

We move our attention to the analysis of the electrical part of the electromechanically coupled problem. As the eigenstrain $\boldsymbol{\gamma}^*$ depends on the electric field vector $\mathbf{E}_2$, it remains to find a solution of the electrical problem. According to the discussion above, we seek a solution that is independent of the axial coordinate x. Hence, the charge equation of

electrostatics reduces to $\nabla_2 \cdot \mathbf{D}_2 = 0$. From Equation (13) the constitutive relation for the in-plane part of the electric displacement vector $\mathbf{D}_2$ follows as

$$\mathbf{D}_2 = \eta \mathbf{E}_2 + \frac{e}{G}\boldsymbol{\tau}, \tag{23}$$

in which we have accounted for the mechanical constitutive relation, $\boldsymbol{\tau} = G\boldsymbol{\gamma} - e\mathbf{E}_2$. $\eta = \in + (ee)/G$ is the permittivity at constant stress. We use the definition of the electric field vector as the negative gradient of a scalar-valued electric potential φ, $\mathbf{E}_2 = -\nabla_2\varphi$, which satisfies the relation $\nabla_2 \times \mathbf{E}_2 = \mathbf{0}$. Noting that $\nabla_2 \cdot \boldsymbol{\tau} = 0$ and substituting Equation (23) into the charge equation, we end up with the following Poisson equation:

$$A: \quad G\eta\Delta_2\varphi = \nabla_2 e \cdot \boldsymbol{\tau}. \tag{24}$$

In order to formulate the boundary conditions, we have to take into account the actual cross-section. The cross-section is a $2b \times 2h$ rectangle in the (y, z)-plane with $-b \leq y \leq b$ and $-h \leq z \leq h$. At the horizontal surfaces electrodes are attached; the lower one has an electric potential V and the upper one is grounded. The vertical surfaces are charge-free, $\mathbf{D}_2 \cdot \mathbf{n} = 0$. Hence, the boundary conditions can be written as

$$\begin{aligned} \partial A: \quad & z = -h : \varphi = V,\ z = h : \varphi = 0, \\ y = \pm b: \ & \mathbf{D}_2 \cdot \mathbf{n} = -\eta\nabla_2\varphi \cdot \mathbf{n} = 0. \end{aligned} \tag{25}$$

Concerning the charge-free boundary conditions the term due to the shear stress vector vanishes, because $\boldsymbol{\tau} \cdot \mathbf{n} = 0$. We seek a decomposition of the solution for φ in the form

$$\varphi = -\frac{V}{2h}(z - h) + \varphi^c. \tag{26}$$

The first part of the solution accounts for inhomogeneous boundary conditions at $z = \pm h$, whereas the second part φ^c is a solution of Equations (24) and (25) with $V = 0$. In the following we will refer to φ^c as the induced electric potential.

3.2.5. *The electromechanical problem in the cross-section*

In the following we summarize the governing equations of the electromechanically coupled problem in the cross-section. First, we discuss the corresponding right-hand sides in some detail. For the mechanical Poisson equation, Equation (18), we obtain

$$G\mathbf{e}_x \cdot \left(\nabla_2 \times \boldsymbol{\gamma}^*\right) = G\mathbf{e}_x \cdot \left(\nabla_2 \times \frac{e}{G}\mathbf{E}_2\right) = \mathbf{e}_x \cdot \left(\nabla_2 \times e\mathbf{E}_2\right), \tag{27}$$

for the second part, because G is constant. The bracketed term can be written as $\nabla_2 \times e\mathbf{E}_2 = \nabla_2 e \times \mathbf{E}_2 + e(\nabla_2 \times \mathbf{E}_2)$. The second term is identically zero. Obviously, the gradient of the piezoelectric coefficient e constitutes the behavior of the solution for the stress function. If it is constant, the eigenstrain has no effect on the stress function. As E_z is the predominant component of the electric field vector, $e = e(y)$ is a reasonable choice. Hence, we find the relation $G\mathbf{e}_x \cdot (\nabla_2 \times \boldsymbol{\gamma}^*) = (de/dy)E_z$. In the case of a bi-morph transducer we

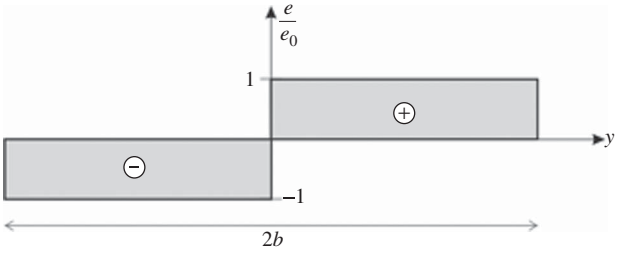

Figure 5. Piezoelectric shear stress coefficient along the torsion actuator width.

have e as shown in Figure 5. For the right-hand side of the electrical Poisson equation, Equation (24), this results in $\nabla_2 e \cdot \boldsymbol{\tau} = (de/dy)\sigma_{xy}$.

Two coupled Poisson equations for ϕ and φ^c with boundary conditions constitute the electromechanically coupled problem in the cross-section. From Equations (18), (24), and (26) and Equations (15) and (25), they are

$$\begin{aligned} A: \quad & \Delta_2\phi = -2G\alpha + \left(\frac{de}{dy}\right)\frac{V}{2h} - \left(\frac{de}{dy}\right)\frac{\partial\varphi^c}{\partial z}, \\ \partial A: \quad & \phi = 0, \\ A: \quad & G\eta\Delta_2\varphi^c = \left(\frac{de}{dy}\right)\frac{\partial\phi}{\partial z}, \\ z = \pm h: \quad & \varphi^c = 0 \quad \textit{and} \quad y = \pm b: \quad \frac{\partial\varphi^c}{\partial y} = 0. \end{aligned} \tag{28}$$

It is interesting to note that the two partial differential equations couple only at the interface of the two oppositely polarized piezoelectric mono-morph actuators. Coupling comes into the play, because the piezoelectric coefficient e changes its sign there. Moreover, the actuation via the applied electric potential difference enters only at this interface as well. In the above formulation this is accounted for in terms of Dirac-delta functions, as $de/dy = 2e_0\delta(y)$.

In the following we will split the solution of the above problem into two parts:

$$\phi = \alpha\phi^\alpha + V\phi^V. \tag{29}$$

The first part accounts for α, whereas the second part accounts for V. ϕ^α and the corresponding induced electric potential $\varphi^{c,\alpha}$ are computed setting $V = 0$ and $\alpha = 1$; accordingly, ϕ^α is a stress function per rate of twist and $\varphi^{c,\alpha}$ is an electric potential per unit rate of twist. ϕ^V and the corresponding $\varphi^{c,V}$ are computed from $V = 1$ and $\alpha = 0$; the latter variables are entities per unit voltage. The significance of this decomposition becomes clear, if we compute the axial moment M_x in a cross-section from the shear stress vector, and hence, from the stress function. We have

$$M_x = \mathbf{M}\cdot\mathbf{e}_x = \mathbf{e}_x \cdot \int_A \mathbf{x}\times\boldsymbol{\tau}\,dA = -\int_A \mathbf{x}\cdot\nabla_2\phi\,dA = 2\int_A \phi\,dA. \tag{30}$$

Note that we have used the identity $\nabla\cdot\mathbf{x} = 2$ and the fact that for a simply connected cross-section $\phi = 0$ holds at the boundary. With the decomposition of Equation (29) we have

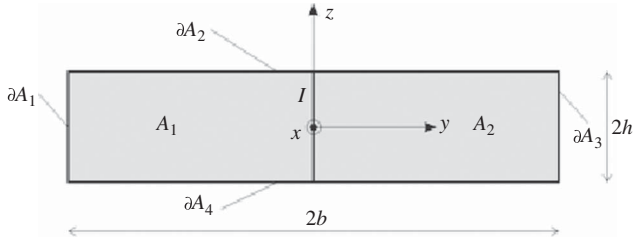

Figure 6. Cross-section of the bi-morph actuator.

$$M_x = 2\int_A \phi dA = \underbrace{\left(2\int_A \phi^{\alpha} dA\right)}_{=(GJ)}\alpha + \underbrace{\left(2\int_A \phi^{V} dA\right)}_{=B} V = (GJ)\frac{d\omega}{dx} + BV. \tag{31}$$

In Equation (31), (GJ) is the torsional stiffness and B is an actuator parameter, which relates the electric potential difference V to the axial moment. For a zero axial moment $M_x = 0$ the rate of twist $\alpha = d\omega/dx$ can be easily computed in statics; it is

$$\alpha = -\frac{B}{(GJ)}V. \tag{32}$$

4. Example

As an example problem, we study the bi-morph actuator made of two oppositely polarized piezoceramic beams. PIC 255 is used as the piezoceramic material; the full set of material parameters can be found in the appendix. The ones we need for the present analysis are given in Table 1. The dimensions of the cross-section, which is shown in Figure 6, are $2b = 0.02$ m and $2h = 0.0005$ m, and the length of the beam is $L = 0.2$ m.One end is clamped and the other one is free. Two solutions are compared to each other: (1) a solution computed using the presented theory, which is independent of the length L; and (2) a solution using three-dimensional finite elements. In particular, we will compare solutions for the rate of twist of the static actuator with an applied voltage difference of $V = 1$ V. Another important aspect will be the study of the significance of electromechanical coupling due to the direct piezoelectric effect, which is accounted for by means of the induced electric potential φ^c.

4.1. The problem in the cross-section

In the following the electromechanically coupled boundary-value problem in the cross-section will be solved by using finite differences. Before we present the solutions, we reformulate the problem of Equation (28) in a form more suitable for implementing a finite difference scheme. Instead of using Dirac-delta functions on the right-hand side, we prefer

Table 1. Material parameters of PIC 255.

G	e_0	$\in$
$22.26 \times 10^9\ Nm^{-2}$	$11.9Cm^{-1}$	$8.234 \times 10^{-9}Fm^{-1}$

to account for their effect in terms of interface conditions at I; see Figure 6. Then we have the following partial differential equations

$$\begin{aligned} A: \quad & \Delta_2 \phi = -2G\alpha \\ & \Delta_2 \varphi^c = 0, \end{aligned} \tag{33}$$

inside the two domains $A = A_1 \cup A_2$. At the surface $\partial A = \partial A_1 \cup \partial A_2 \cup \partial A_3 \cup \partial A_4$ we have

$$\begin{aligned} & \partial A: \quad \phi = 0, \\ & \partial A_2 \cup \partial A_4: \quad \varphi^c = 0 \quad \textit{and} \quad \partial A_1 \cup \partial A_3: \quad \frac{\partial \varphi^c}{\partial y} = 0. \end{aligned} \tag{34}$$

At the interface I certain continuity conditions must be satisfied. The shear stress σ_{xy} must be continuous; hence, its jump $[\![\sigma_{xy}]\!]$ must be zero. Here, σ_{xy} follows from the definition of the stress function as $\sigma_{xy} = \partial\phi/\partial z$. As the jump of an entity $[\![.]\!]$ and the tangential derivative at the interface can be interchanged, we find that the jump of the stress function at the interface must be constant with respect to the height of the bi-morph; furthermore, this jump is zero at $z = \pm h$, from which we conclude on the continuity of the stress function, $[\![\phi]\!] = 0$, at the interface. Next, we note that the tangential component of the electric field vector must also be continuous, $[\![E_z]\!] = 0$. Using the relation $E_z = -\partial\varphi/\partial z$ and following our previous argument, we derive the continuity of the electric potential, $[\![\varphi]\!] = 0$ at the interface. According to Equation (26) the electric potential is composed of two parts. The one from the electric potential difference is automatically continuous due to the equipotential area condition at the electrodes; even in the case when two separate electrodes for the two oppositely polarized beams were used, the fact that the applied electric potential is identical at the two separate electrodes is sufficient for continuity of the electric potential difference. The second part of the electric potential φ^c then must satisfy $[\![\varphi^c]\!] = 0$. The third condition at the interface results from the continuity of the normal component of the electric displacement vector, $[\![D_y]\!] = 0$. For a reformulation we use the constitutive relation $D_y = \eta E_y + (e/G)\sigma_{xy}$. Therefore, we have

$$[\![D_y]\!] = \eta\,[\![E_y]\!] + [\![e]\!]\,\frac{\sigma_{xy}}{G} = 0, \tag{35}$$

because η, G and σ_{xy} are continuous. Using $E_y = -\partial\varphi^c/\partial y$ and $\sigma_{xy} = \partial\phi/\partial z$, we find

$$G\eta\left[\!\left[\frac{\partial \varphi^c}{\partial y}\right]\!\right] = [\![e]\!]\,\frac{\partial \phi}{\partial z}. \tag{36}$$

Finally, we have continuity of the shear strain $[\![\gamma_{xz}]\!] = 0$, which follows from the compatibility conditions. We insert the constitutive relation $\gamma_{xz} = \sigma_{xz}/G + (e/G)E_z$ and obtain

$$G\,[\![\gamma_{xz}]\!] = [\![\sigma_{xz}]\!] + [\![e]\!]\,E_z = 0. \tag{37}$$

This result follows from the continuity of G and E_z. With $E_z = V/(2h) - \partial\varphi^c/\partial z$ and $\sigma_{xz} = -\partial\phi/\partial y$ we end up with

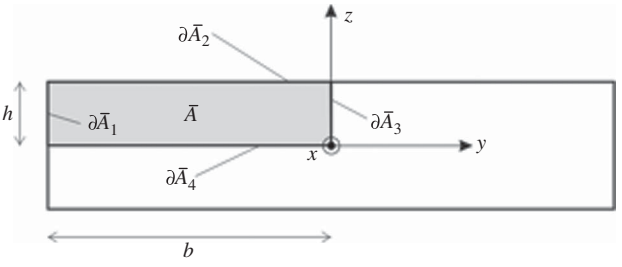

Figure 7. Quarter of the cross-section of the bi-morph actuator.

$$\left[\left[\frac{\partial\phi}{\partial y}\right]\right] = [\![e]\!]\left(\frac{V}{2h} - \frac{\partial\varphi^c}{\partial z}\right). \tag{38}$$

For the bi-morph transducer we have $[\![e]\!] = 2e_0$. We summarize the interface conditions at I; they are:

$$[\![\phi]\!] = 0, \ \left[\left[\frac{\partial\phi}{\partial y}\right]\right] = 2e_0\left(\frac{V}{2h} - \frac{\partial\varphi^c}{\partial z}\right), \ [\![\varphi^c]\!] = 0, \ G\eta\left[\left[\frac{\partial\varphi^c}{\partial y}\right]\right] = 2e_0\frac{\partial\phi}{\partial z}. \tag{39}$$

Equations (33), (34) and (39) constitute the electromechanically coupled problem in the cross-section.

Computing solutions of this problem one will find that the stress function ϕ is symmetric with respect to both the y and z coordinates. In contrast, φ^c is only symmetric with respect to y, but skew-symmetric with respect to z. This latter fact may also be concluded from the coupled boundary-value problem itself. Hence, it is not necessary to solve the problem in the whole domain $2b \times 2h$, but only in a quarter of the domain. If we use the upper left quarter (see Figure 7), we can easily formulate the corresponding electromechanically coupled boundary-value problem. It reads:

$$\bar{A}: \quad \Delta_2\phi = -2G\alpha,$$

$$\Delta_2\varphi^c = 0 \tag{40}$$

and

$$\partial\bar{A}_1: \quad \phi = 0 \quad \textit{and} \quad \frac{\partial\varphi^c}{\partial y} = 0,$$

$$\partial\bar{A}_2: \quad \phi = 0 \quad \textit{and} \quad \varphi^c = 0,$$

$$\partial\bar{A}_3: \quad \frac{\partial\phi}{\partial y} = -e_0\left(\frac{V}{2h} - \frac{\partial\varphi^c}{\partial z}\right) \quad \textit{and} \quad \frac{\partial\varphi^c}{\partial y} = -\frac{e_0}{G\eta}\frac{\partial\phi}{\partial z},$$

$$\partial\bar{A}_4: \quad \frac{\partial\phi}{\partial z} = 0 \quad \textit{and} \quad \varphi^c = 0. \tag{41}$$

Equations (40) and (41) represent the problem in the cross-section, for which we will be presenting numerical solutions using finite differences in the following.

4.2. Finite difference solution

The unknown functions $\phi(y,z)$ and $\varphi^c(y,z)$ are projected onto a grid consisting of nodes (y_i, z_j). The numerical scheme allows one to calculate approximate values $\phi_{i,j}$ and $\varphi^c_{i,j}$ at the nodes; the functions can then be reconstructed by interpolation, and the integral characteristics are calculated from the nodal values using standard methods of computational mathematics.

Inside the domain $h \times b$ we choose a simple regular grid with N_z nodes for the thickness h and $N_y = (b/h)(N_z + 1) - 1$ nodes for the width b. As the number of spans equals the number of nodes inside the domain plus 1, the dimensions of the spans in the two directions h_y and h_z are identical and we compute them from

$$h_y = \frac{b}{N_y + 1} = \frac{h}{N_z + 1} = h_z. \tag{42}$$

We use the index i for the width and the index j for the thickness; nodes are then identified by a pair of indices (i,j). Here i runs from $i_{start} = 0$ to $i_{end} = N_y + 1$ and j runs from $j_{start} = 0$ to $j_{end} = N_z + 1$. The partial differential equations, Equation (40), are approximated by difference equations, which are

$$\frac{1}{h_y^2}\left(\phi_{i+1,j} - 2\phi_{i,j} + \phi_{i-1,j}\right) + \frac{1}{h_z^2}\left(\phi_{i,j+1} - 2\phi_{i,j} + \phi_{i,j-1}\right) = -2G\alpha,$$

$$\frac{1}{h_y^2}\left(\varphi^c_{i+1,j} - 2\varphi^c_{i,j} + \varphi^c_{i-1,j}\right) + \frac{1}{h_z^2}\left(\varphi^c_{i,j+1} - 2\varphi^c_{i,j} + \varphi^c_{i,j-1}\right) = 0. \tag{43}$$

Here, the range of indices is $i = i_{start} + 1, \ldots, i_{end} - 1$ and $j = j_{start} + 1, \ldots, j_{end} - 1$. Hence, the number of equations is identical to twice the number of nodes inside the domain $2(N_y \times N_z)$. The number of unknowns is $2[(N_y + 2) \times (N_z + 2)]$, which is larger than the number of equations so far. The missing equations follow from the boundary conditions. The homogeneous Dirichlet and Neumann boundary conditions from Equation (41) at $\partial\bar{A}_1$, $\partial\bar{A}_2$ and $\partial\bar{A}_4$ can be easily formulated. We have

$$\begin{aligned}
\partial\bar{A}_1: &\quad \phi_{i_{start},j} = 0\,, \quad \varphi^c_{i_{start}+1,j} - \varphi^c_{i_{start},j} = 0,\\
\partial\bar{A}_2: &\quad \phi_{i,j_{end}} = 0\,, \quad \varphi^c_{i,j_{end}} = 0,\\
\partial\bar{A}_4: &\quad \phi_{i,j_{start}+1} - \phi_{i,j_{start}} = 0\,, \quad \varphi^c_{i,j_{start}} = 0.
\end{aligned} \tag{44}$$

Here, the index j runs from $j = j_{start} + 1, \ldots, j_{end} - 1$ and the index i from $i = i_{start}, \ldots, i_{end}$. Finally, the remaining $2(j_{end} - 1)$ equations are the boundary conditions at $\partial\bar{A}_3$; the latter are formulated according to

$$\frac{\phi_{i_{end},j} - \phi_{i_{end}-1,j}}{h_y} = -e_0\left(\frac{V}{2h} - \frac{\varphi^c_{i_{end},j+1} - \varphi^c_{i_{end},j-1}}{2h_z}\right),$$

$$\frac{\varphi^c_{i_{end},j} - \varphi^c_{i_{end}-1,j}}{h_y} = -\frac{e_0}{G\eta}\frac{\phi_{i_{end},j+1} - \phi_{i_{end},j-1}}{2h_z}. \tag{45}$$

with j running from $j = j_{start} + 1, \ldots, j_{end} - 1$. Hence, the number of unknowns and the number of equations are identical and the problem can be solved. In our case, we have implemented these equations in Mathematica®.

As mentioned earlier we solve the problem twice. First, for $\alpha = 1$ and $V = 0$, from which we compute ϕ^{α} and the corresponding $\varphi^{c,\alpha}$; secondly, for $\alpha = 0$ and $V = 1$, from which we compute ϕ^{V} and the corresponding $\varphi^{c,V}$. The results are shown in Figures 8 and 9. In these figures, we present a solution in which we use $N_z = 64$ and accordingly

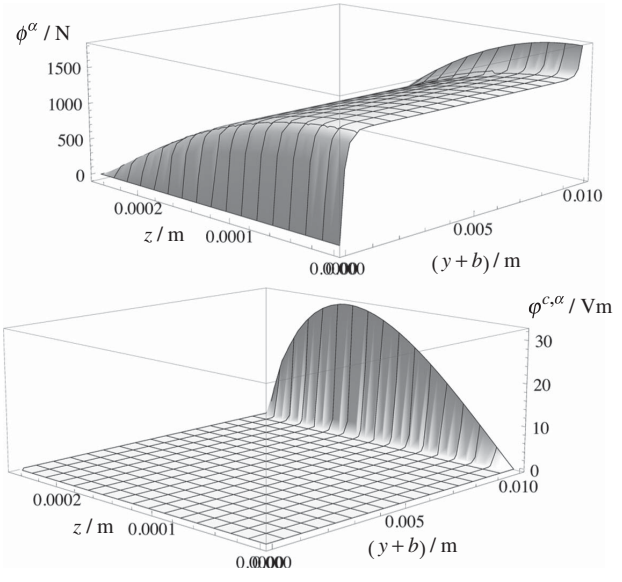

Figure 8. Mechanical stress function ϕ^{α} and corresponding induced electric potential $\varphi^{c,\alpha}$ per unit rate of twist.

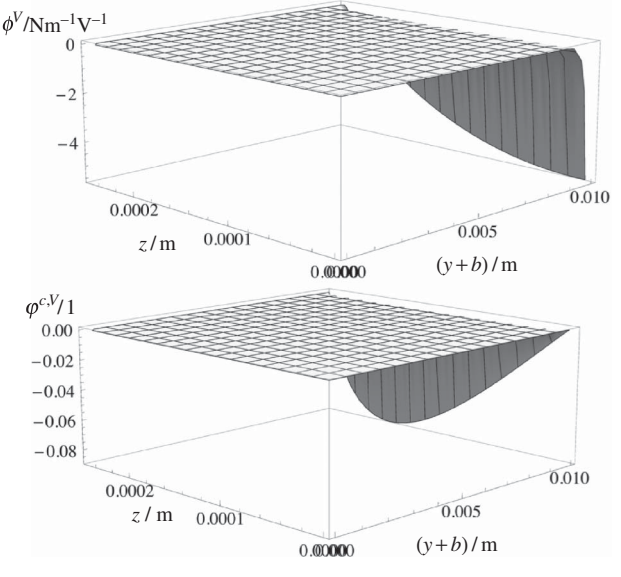

Figure 9. Electric stress function ϕ^{V} and corresponding induced electric potential $\varphi^{c,V}$ per unit voltage.

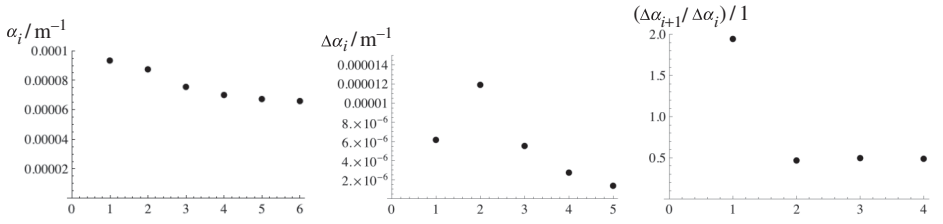

Figure 10. Convergence for rate of twist (left), difference between subsequent values of the rate of twist (center) and ratio between subsequent differences (right).

$N_y = 40(N_z + 1) - 1 = 2599$. Concerning the convergence of the solution we have conducted a study in which we have used $N_z = (2, 4, 8, 16, 32, 64)$. For each solution the rate of twist $\alpha = -BV/(GJ)$ for a potential difference $V = 1$ V has been computed; the results for the six values are shown in the left plot of Figure 10. The five differences between subsequent values $\Delta\alpha_i = \alpha_{i+1} - \alpha_i$ are shown in the center of Figure 10, and the right plot presents the four ratios between subsequent differences, $\Delta\alpha_{i+1}/\Delta\alpha_i$. Obviously, the solution converges, the difference between subsequent solutions tends to zero and the ratio between subsequent differences tends to a value of 0.5; hence, we have quadratic convergence. The final results ($N_z = 64$) for the parameters (GJ), B and for α are given in Table 2. One can see that the electromechanically coupled solution (EM coupled) results in significant differences compared to a solution not taking this coupling into account; the latter assumes the electric potential to be $\varphi = -\frac{V}{2h}(z - h)$. Hence, the effect of the induced potential φ^c due to the direct piezoelectric effect on the mechanical behavior is neglected, or according to Tiersten [31] we are using the approximation denoted as *small piezoelectric coupling*. In our problem such an approximation can clearly not be used. In contrast to B and α the torsional stiffness (GJ) is only slightly affected by this coupling; in particular, the torsional stiffness is higher in the coupled solution. This is a well-known fact that has been studied and analyzed in the literature; see, e.g. Krommer [32, 33] and Vetyukov *et al*. [34] for the case of beam and plate bending with embedded or attached piezoceramics exhibiting the d_{31}-effect.

4.3. Numerical validation

As we have found that the electromechanical coupling has a strong effect on the behavior of the bi-morph, it is near at hand to verify such a result by means of a comparison to electromechanically coupled three-dimensional finite element computations. We use ABAQUS® for this purpose.

We recall that we study a bi-morph actuator with width $2b = 0.02$m, thickness $2h = 0.0005$m and length $L = 0.2$m. At $x = 0$m the actuator is clamped and at $x = L$ it is free.

Table 2. Structural material parameters and rate of twist α for a bi-morph actuator: Electromechanically coupled vs. decoupled theory

	(GJ)/Nm^2	B/NmV^{-1}	α/m^{-1}
EM coupled	18.12×10^{-3}	-1.1906×10^{-6}	65.72×10^{-6}
decoupled	18.05×10^{-3}	-0.9927×10^{-6}	55.00×10^{-6}
Error	3.86%	16.62%	16.31%

Table 3. Rate of twist α for bi-morph transducer: Comparison to 3D FE

	α/m^{-1} (EM coupled)	α/m^{-1} (decoupled)	Error
Present	65.72×10^{-6}	55.00×10^{-6}	16.3%
ABAQUS®	63.52×10^{-6}	57.00×10^{-6}	10.3%
Error	3.35%	−3.64%	

We use C3D20E piezoelectric quadratic (20 nodes) brick elements with 400 elements along the length, 40 elements along the width and 10 elements through the thickness. The opposite polarization of the two piezoceramic beams (see Figure 3) is implemented by changing the sign of the piezoelectric stress coefficients to be negative. For this purpose, two different sets of piezoelectric properties and two sections are assigned to the two piezoceramic beams. The material properties for the piezoceramic material PIC 255 are given in the appendix. For the actuator problem we are studying, electrodes are implemented by prescribing the electric potential at all nodes at the top horizontal surface as zero and the electric potential at all nodes at the bottom horizontal surface as $V = 1$ V.

We are in particular interested in a comparison of result for the rate of twist. We compute the latter from the maximum vertical displacement u_z^{max}, which is the vertical displacement at $x = L$, $y = b$ and $z = 0$m. From this displacement we find

$$\alpha^{FE} = \frac{u_z^{max}}{bL}. \tag{46}$$

In Table 3 the results from the present theory are compared with those computed with ABAQUS®. Two cases are presented: (1) the electromechanically coupled one (EM coupled) and (2) a case for which the induced electric potential is neglected (decoupled). The latter was already discussed with respect to its implementation in the present theory. In the finite element solution this decoupled solution can be computed by increasing the permittivities at constant strain; we have used a factor 100 as it has turned out that a further increase has no more effect. We see from the results for the rate of twist that the deviations are within ±4% for both the electromechanically coupled and the decoupled solution, which is within an acceptable range. Concerning the effect of electromechanical coupling by means of the induced electric potential, we see that the significance of this effect is validated by the finite element solution. It is smaller than in the present theory; yet, it is clearly an effect that cannot be neglected.

5. Conclusions and perspectives

In this paper we have presented a thorough mathematical analysis for the problem of a bi-morph d_{15} piezoelectric actuator. The derived solution represents an exact solution of the electromechanically coupled 3D problem under the condition that the solution is independent of the axial coordinate. A finite difference solution was implemented and it was shown that the so-called induced electric potential has a significant effect on the actuated rate of twist. Finally, this latter result was verified by a comparison to a solution computed using electromechanically coupled 3D finite elements. For the future we intend to tackle some open problems of our analysis, which are:

- The extension of the presented theory with respect to the computation of the warping function to answer the question of whether the warping function for the piezoelastic problem is identical to the elastic one.
- The analysis of the effect of the boundary conditions, which are not satisfied by the presented solution in order to estimate the range of validity of the latter solution.
- The extension of the presented analysis to the case of a bi-morph piezoceramic core sandwiched by two face layers in order to put a bi-morph d_{15} actuator into practice.

Moreover, the integration of such a device into a composite structure will require extended modeling with respect to the dynamic behavior and the sensing effect as well as the necessary model reduction in order to provide a sufficiently simple, yet accurate model for control applications. The result of this paper will serve as the basis for future models for smart structures with embedded d_{15} actuators and sensors.

Acknowledgments

Support of the present work in the framework of the Comet K2 *Austrian Center of Competence in Mechatronics (ACCM)* is gratefully acknowledged.

References

[1] E.F. Crawley, *Intelligent structures for aerospace – A technology overview and assessment*, AIAA J. 32 (1994), pp. 1689–1699.
[2] I. Chopra, *Review of state of art of smart structures and integrated systems*, AIAA J. 40 (2002), pp. 2145–2187.
[3] S.S. Rao and M. Sunar, *Piezoelectricity and its use in disturbance sensing and control of flexible structures: a survey*, Appl. Mech. Rev. 47 (1994), pp. 113–123.
[4] W.P. Mason, *Piezoelectricity, its history and applications*, J. Acoust. Soc. Amer. 6 (1981), pp. 1561–1566.
[5] J. Yang, *An Introduction to the Theory of Piezoelectricity*, Springer, Berlin, 2005.
[6] T. Mura, *Micromechanics of Defects in Solids*, Kluwer Academic Publishers, Dordrecht, 1991.
[7] H. Irschik, M. Krommer, A.K. Belyaev, and K. Schlacher, *Shaping of piezoelectric sensors/actuators for vibrations of slender beams: coupled theory and inappropriate shape functions*, J. Intell. Mater. Syst. Struct. 9 (1998), pp. 546–554.
[8] O.J. Aldraihem and R.C. Wetherhold, *Mechanics and control of coupled bending and twisting vibration of laminated beams*, Smart Mater. Struct. 6 (1997), pp. 123–133.
[9] H. Kioua and S. Mirza, *Piezoelectric induced bending and twisting of laminated composite shallow shells*, Smart Mater. Struct. 9 (2000), pp. 476–484.
[10] M.L. Zhu, S.W.R. Lee, H.L. Li, T.Y. Zhang, and P. Tong, *Modeling of torsional vibration induced by extension-twisting coupling of anisotropic composite laminates with piezoelectric actuators*, Smart Mater. Struct. 11 (2002), pp. 55–62.
[11] C. Zehetner, *Compensation of torsional vibrations in rods by piezoelectric actuation*, Acta Mechanica 207 (2009), pp. 121–133.
[12] C. Zehetner and M. Krommer, *Control of torsional vibrations in piezolaminated rods*, Struct. Control Health Monitor. 2011; doi: 10.1002/stc.455.
[13] H.S. Tzou, R. Ye, and J.H. Ding, *A new X-actuator design for dual bending/twisting control of wings*, J. Sound Vibr. 82 (2008), pp. 36–49.
[14] Z.C. Qiu, H.X. Wu, and D. Zhang, *Experimental researches on sliding mode active vibration control of flexible piezoelectric cantilever plate integrated gyroscope*, Thin-Walled Struct. 47 (2009), pp. 836–846.
[15] A. Benjeddou, *Shear-mode piezoceramic advanced materials and structures: a state of the art*, Mech. Adv. Mater. Struct. 14 (2007), pp. 263–275.
[16] C. Sung, V.V. Varadan, X. Bao, and V.K. Varadan, *Active torsional vibration control experiments using shear type piezoceramic sensors and actuators*, J. Intell. Mater. Syst. Struct. 4 (1994), pp. 436–442.

[17] A.E. Glazounov, Q.M. Zhang, and J.S. Kim, *Torsional actuator and stepper motor based on piezoelectric d_{15} shear response*, J. Intell. Mater. Syst. Struct. 11 (2000), pp. 456–468.
[18] L.R. Centolanza, E.C. Smith, and B. Munsky, *Induced-shear piezoelectric actuators for rotor blade trailing edge flaps*, Smart Mater. Struct. 11 (2002), pp. 24–35.
[19] D. Thakkar and R. Ganguli, *Helicopter vibration reduction in forward flight with induced-shear based piezoceramic actuation*, Smart Mater. Struct. 13 (2004), pp. 599–608.
[20] O.M. Pawar and S.N. Jung, *Single-crystal-material-based induced-shear actuation for vibration reduction of helicopters with composite rotor systems*, Smart Mater. Struct. 17 (2008), 065009.
[21] A. Butz, S. Klinkel, and W. Wagner, *A piezoelectric 3D-beam finite element formulation accounting for geometrical and material nonlinearities*, Internal Research Report, University of Karlsruhe, 2007.
[22] P. Berik and A. Benjeddou, *Piezoelectric d_{15} shear response-based torsion actuation mechanism: an experimental benchmark and its 3D finite element simulation*, Internat. J. Smart Nano Mater. 1 (2010), pp. 224–235.
[23] A.I. Lurie, *Analytical Mechanics*, Springer, Berlin, 2002.
[24] H. Reissner, *Selbstspannungen elastischer Gebilde*, Zeitschrift für Angewandte Mathematik und Mechanik 11 (1931), pp. 59–70.
[25] P. Nemenyi, *Eigenspannungen und Eigenspannungsquellen*, Zeitschrift für Angewandte Mathematik und Mechanik 11 (1931), pp. 1–8.
[26] J.R. Vinson, *The Behavior of Shells Composed of Isotropic and Composite Materials*, Kluwer, Dordrecht, 1993.
[27] R.B. Hetnarski, *Basic equations of the theory of thermal stresses*, in *Thermal Stresses I*, R.B. Hetnarski, ed., North-Holland, Amsterdam, 1991.
[28] P. Berik and A. Benjeddou, *Static experimentations of the piezoceramic d_{15}-shear actuation mechanism for sandwich structures with opposite or same poled patches- assembled core and composite faces*. International Journal of Smart and Nano Materials 2(4) (2011), pp. 230–244.
[29] V. Eliseev, *Mechanics of Deformable Solid Bodies* (in Russian), St. Petersburg State Polytechnic University Publishing House, 2006.
[30] F. Ziegler, *Mechanics of Solids and Fluids*, Springer, New York, 1998.
[31] H.F. Tiersten, *Linear Piezoelectric Plate Vibrations*, Plenum, New York, 1969.
[32] M. Krommer, *On the correction of the Bernoulli–Euler beam theory for smart piezoelectric beams*, Smart Mater. Struct. 10 (2001), pp. 668–680.
[33] M. Krommer, *The significance of non-local constitutive relations for composite thin plates including piezoelastic layers with prescribed electric charge*, Smart Mater. Struct. 12 (2003), pp. 318–330.
[34] Y. Vetyukov, A. Kuzin, and M. Krommer, *Asymptotic splitting in the three-dimensional problem of elasticity for non-homogeneous piezoelectric plates*, Internat. J. Solids Struct. 48 (2011), pp. 12–23.

Appendix: Material parameters of PIC 255

The material parameters (in the form of engineering constants for the elastic parameters) for the piezoceramic material PIC 255 with the polarization in the 3-direction are given in Table 4. Piezoelectric stress coefficients and permittivities at constant strain needed for the constitutive relations of Equation (2) are those given in Table 4. The components of the fourth-rank tensor **C** as introduced in Equation (2) can be computed from the engineering constants; they are given in Table 5.

Table 4. Material parameters of PIC 255.

Constant	Notation	Value
Piezoelectric stress coefficients / Cm^{-2}	$e_{31} = e_{32}$	−7.15
	e_{33}	13.7
	$e_{15} = e_{24}$	11.9
Permittivities at constant strain / nFm^{-1}	$\in_{11}=\in_{22}$	8.234
	$\in_{33}$	7.588
Young's moduli / GNm^{-2}	$E_1 = E_2$	62.89
	E_3	47.69
Shear moduli / GNm^{-2}	$G_{13} = G_{23}$	22.26
	G_{12}	23.15
Poisson ratios / 1	$\nu_{13} = \nu_{23}$	0.46
	ν_{12}	0.36

Table 5. Elasticity moduli of PIC 255.

Elasticity moduli / GNm^{-2}	C_{11}	C_{33}	C_{12}	C_{13}	C_{55}	C_{66}
Value	121.7	95.65	75.43	68.75	22.26	23.15